ACS Catalysis

Research Article

pubs.acs.org/acscatalysis

Amine-Functionalized GO as an Active and Reusable Acid–Base Bifunctional Catalyst for One-Pot Cascade Reactions

Fang Zhang,* Huangyong Jiang, Xiaoyan Li, Xiaotao Wu, and Hexing Li*

The Education Ministry Key Lab of Resource Chemistry and Shanghai Key Laboratory of Rare Earth Functional Materials, Shanghai Normal University, Shanghai 200234, People's Republic of China

Supporting Information

ABSTRACT: The amine-functionalized graphene oxide was prepared by a facile one-step silylation approach and used as an acid–base bifunctional catalyst in one-pot cascade reactions containing successive acetal hydrolysis and Knoevenagel condensation owing to the separate coexistence of original carboxylic acid on the edge of the GO sheet and the postgrafted amine groups on the GO basal surface. This catalyst exhibited much higher activity than either amine-functionalized active carbon, amine-functionalized SBA-15, or amine-functionalized Al_2O_3 due to the enriched surface acid sites and the diminished diffusion limitation as well as high catalyst dispersion in liquid solution due to the unique two-dimensional structure. More importantly, this catalyst could be easily recycled and used repetitively, showing potential application in industry.

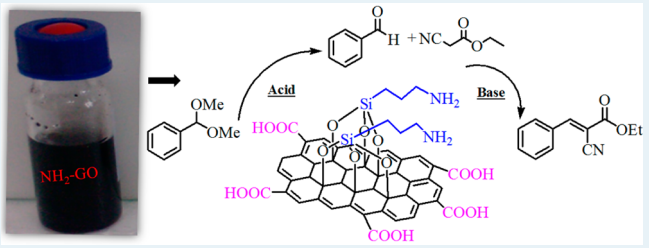

KEYWORDS: *acid–base bifunctional catalyst, one-pot cascade reactions, acetal hydrolysis, Knoevenagel condensation, amine-functionalized graphene oxide*

INTRODUCTION

The unparallel ability of enzymes to realize the complicated but efficient metabolic processes is mostly through highly specific but multistep synergic catalytic processes.[1] However, the present industrial production of fine chemicals and pharmaceuticals usually needs iterative synthetic strategies,[2] which are time- and cost-demanding as well as waste-producing.[3] "One-pot" cascade reactions represent the development trend of modern organic synthesis owing to the simplified process with low cost and reduced waste.[4] Until now, most studies have focused on homogeneous catalysts.[5] Despite the high activity and selectivity, homogeneous catalysts are difficult to recycle and reuse, which will inevitably enhance the cost and even cause pollution of the environment and/or final product by heavy metallic ions.[6] Heterogeneous catalysts are easily recycled and reused.[7] More importantly, the immobilized active sites could avoid their cross-poisoning effect.[8] The key problem is the poor catalytic efficiency due to the reduced dispersion of active sites, the enhanced diffusion limit, and the damaged chemical microenvironment of the active center.

The combination of acid and base catalysts for the cascade process is recognized as a more attractive approach since the acidic and basic functions can activate electrophiles and nucleophiles, respectively.[9] Obviously, such cascade reactions could not be performed in one pot by using homogeneous catalysts due to the acid–base neutralization, but they could be realized by using heterogeneous catalysts since the acid and base groups are fixed and cannot contact directly.[10] To date, acid–base bifunctional catalysts hosted in the solid matrix, such as silica, clay, and polymer, *etc.*, have been reported,[11] but they often suffer from tedious protection–deprotection procedures and/or exhibit unsatisfactory catalytic efficiencies due to the enhanced steric hindrance and the change of the chemical microenvironment, mainly due to the weak surface acidity.[12−14]

Recently, graphene has received increasing interest owing to its unique structural and surface properties.[15] Accordingly, a graphene derivative, such as graphene oxide, offers a wide range of possibilities to synthesize the novel functional catalysts owing to its abundant oxygen-containing functionalities.[16] The structure of graphene oxide sheets consists of a basal plane of the sheet, decorated with hydroxyl and epoxy functional groups, while carbonyl groups are present as carboxylic acids along the sheet edge. Recently, several research groups successfully demonstrated that GO could be an ideal carbocatalyst for use in a variety of chemical transformations such as hydration, oxidation, C–H activation, and polymerization.[17] Up to now, GO has been used only as a monofunctional catalyst based on its intrinsic chemical properties of either high acidity or strong oxidization. Herein, we report for the first time a novel acid–base bifunctional catalyst by using the intrinsic carboxylic acids on the edges of GO and the amine groups postgrafted onto the GO basal surface (see Scheme 1), which exhibited excellent activity in one-pot deacetalization–Knoevenagel cascade reactions owing to the unique two-dimensional structure with low mass transfer limitation and suitable surface acidity of GO. Meanwhile, it could be easily recycled and reused repetitively.

Received: September 2, 2013
Revised: November 18, 2013

   dx.doi.org/10.1021/cs400761r | *ACS Catal.* 2014, 4, 394–401

Scheme 1. Illustration of the Amine-Functionalized Graphene Oxide Preparation

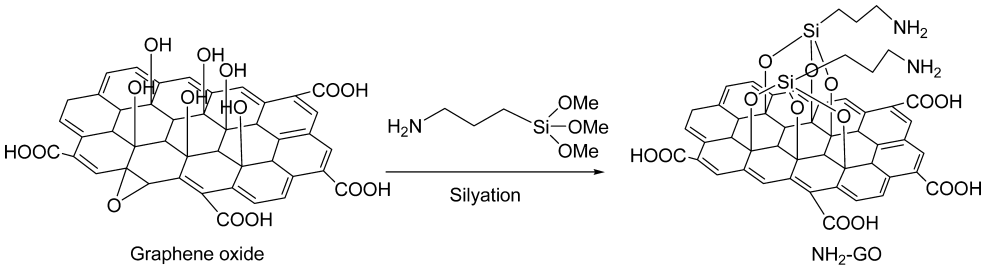

EXPERIMENTAL PROCEDURES

Catalyst Preparation. The parent graphene oxide (GO) was prepared by the previously reported Hummers method.[18] Then, 0.50 g of GO was dispersed in 20 mL of anhydrous toluene. After ultrasonication for 2.0 h, a certain amount of 3-aminopropyltriethoxysilane (APTES) was added and stirred for 12 h via reflux. The solid was collected by filtration, washed with dichloromethane, and vacuum-dried at 60 °C for 10 h. The final catalyst could be defined as amine-functionalized graphene oxide: NH_2-GO-1, NH_2-GO-2, and NH_2-GO-3, corresponding to 100, 200, and 400 μL of APTES used in the initial mixture, respectively.

For comparison, the NH_2-AC was also synthesized according to the following procedure. One gram of activated carbon (AC) was mixed with 40 mL of concentrated nitric acid and stirred at 80 °C for 2.0 h. Then the mixture was filtered and washed with ethanol, followed by grafting amine groups according to the aforementioned way using 200 μL of APTES for 0.50 g of AC. The NH_2-SBA-15 was prepared by directly grafting amine groups onto the SBA-15[19] according to the aforementioned way using 200 μL of APTES for 0.50 g of SBA-15. The NH_2-Al_2O_3 was prepared through the same procedure with the NH_2-SBA-15 sample.

The control samples acidified NH_2-GO-2 (NH_2-GO-2-A) and basified NH_2-GO-2 (NH_2-GO-2-B) were prepared by immersing NH_2-GO-2 in 1.0 mol/L HCl and NaOH aqueous solution for 1.0 h, respectively. The obtained solid powders were washed by water and dried in vacuum at 60 °C for 10 h, resulting in the final product.

Characterization. The nitrogen, silicon, carbon, and hydrogen contents were determined in a Vario EL III elemental analysis analyzer. Fourier transform infrared spectroscopy (FTIR) spectra were collected through a Nicolet Magna 550 spectrometer using the standard KBr pellet method. Solid-state ^{13}C CP MAS NMR, ^{15}N CP MAS NMR, and ^{29}Si MAS NMR spectra were recorded on a Bruker AV-400 spectrometer using 100.6, 40.5, and 79.5 MHz, respectively. Thermogravimetric analysis (TGA) was carried out on Shimadzu DTG-60 thermogravimetric analyzer with a ramping rate of 10 °C/min in 50 mL/min of nitrogen flow. The surface electronic states were analyzed by X-ray photoelectron spectroscopy (XPS, Perkin-Elmer PHI 5000C ESCA). All the binding energy values were calibrated by using C_{1S} = 284.6 eV as a reference. X-ray diffractions (XRD) were performed on a Rigaku D/MAX B diffraction system with Cu Kα radiation. Atomic force microscope (AFM) images were observed through a Multimode IIIa electron microscope. Scanning electron microscopy (SEM) and transmission electron microscopy (TEM) images were obtained on a JSM-6380LV electron microscope and a JEOL JEM2011 electron microscope, respectively. The temperature-programmed desorption of ammonia (NH_3-TPD) experiments was performed on flow apparatus (Micrometrics TP-5080). The samples were saturated with a pure NH_3 flow, and then the physisorbed NH_3 was removed through purging with argon gas at 40 °C for 0.5 h. The sample was then heated to 750 °C at a speed of 10 °C/min. The amounts of acidic site were measured by calculating the ammonia absorption per gram of the samples through a TCD detector.

Activity Test. One-pot cascade reactions were carried out in a 10 mL round-bottomed flask. In a typical run of reactions, a catalyst containing 0.040 mmol nitrogen species, 0.50 mmol benzaldehyde dimethyl acetal, 0.60 mmol ethyl cyanoacetate, 5.0 mL anhydrous toluene, and 50 μL water was mixed and allowed to stir at 80 °C for 3.0 h. The product analysis was performed on a high-performance liquid chromatograph with mass spectrometry (HPLC/MS, Agilent 6410B). The reaction conversion was calculated based on benzaldehyde dimethyl acetal since there was excess ethyl cyanoacetate. The reproducibility was checked by repeating experiments at least three times and was found to be within acceptable limits (±5%).

In order to determine the catalyst durability, the catalyst was centrifuged after each run of the reactions and the clear supernatant liquid was decanted slowly. The residual solid catalyst was washed thoroughly with toluene and dichloromethane, followed by vacuum drying at 80 °C for 6.0 h. Then, the catalyst was reused with a fresh charge of solvent and reactants for subsequent recycle runs under the same reaction conditions.

RESULTS AND DISCUSSION

Structural Characteristics. As shown in Table 1, the nitrogen loading increased up to 2.3 wt % after amino-silylation with the enhanced APTES amount, indicating the successful immobilization of amine groups onto the GO. Meanwhile, the mole ratios between nitrogen and silicon content of NH_2-GO, NH_2-AC, and NH_2-Al_2O_3 samples were close to 1:1, which indicated that there were no other nitrogen sources

Table 1. Elemental Analysis of GO and Amine-Functionalized GO, AC, SBA-15, and Al_2O_3

sample	C (wt %)	H (wt %)	N (wt %)	Si (wt %)	mole ratio (N/Si)
GO	52	1.8	0	0	
NH_2-GO-1	48	1.9	0.53	1.1	1:1.01
NH_2-GO-2	46	2.0	1.0	2.2	1:1.05
NH_2-GO-3	45	2.1	2.3	4.9	1:1.06
NH_2-AC	74	1.6	1.0	2.1	1:1.05
NH_2-SBA-15	2.7	2.1	1.1		
NH_2-Al_2O_3	3.3	1.8	1.3	2.7	1:1.03

dx.doi.org/10.1021/cs400761r | ACS Catal. 2014, 4, 394−401

contaminating these samples in our catalyst preparation process. The existence of amine species could be further confirmed by FTIR and NMR. The FTIR spectra in Figure 1

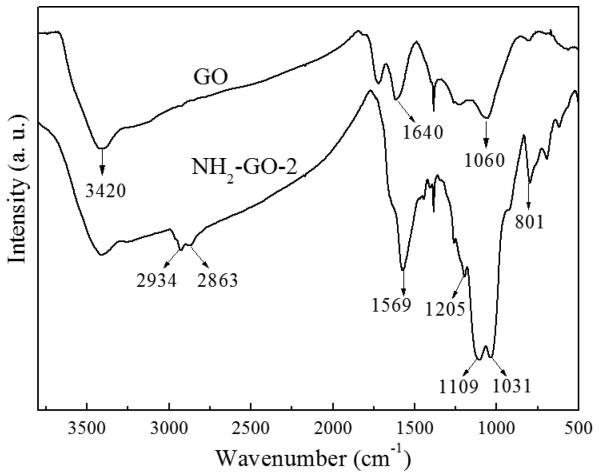

Figure 1. FTIR spectra of GO and NH_2-GO-2 samples.

revealed that the pristine GO displayed three peaks at 3420, 1640, and 1060 cm^{-1} characteristic of the hydroxyl, carboxyl, and epoxy groups, respectively.[20] The representative NH_2-GO-2 exhibited two additional peaks at 2934 and 2863 cm^{-1}, indicative of the asymmetric and symmetric stretching modes of C−H bonds from CH_2−CH_2 groups connecting with the NH_2 group. Two other additional peaks at 1569 and 801 cm^{-1} could be ascribed to the symmetric N−H stretching band and the N−H out-of-plane bending vibration from the NH_2 group, respectively.[21] Besides, the appearance of two new peaks at 1109 and 1031 cm^{-1} were assigned to the Si−O−Si asymmetric stretching and Si−O−C stretching vibration.[22] Moreover, the intensity of the absorption peak around 3400 cm^{-1} characteristic of the surface OH groups significantly decreased, suggesting that the amino-silylation mainly occurred via reaction with surface OH. As shown in Figure 2, the ^{29}Si MAS NMR spectrum of NH_2-GO-2 displayed one intense peak at 66 ppm corresponding to the T^3 signal (T^3 = $RSi(OSi)_3$),[23] indicating that the Si species were covalently bonded with GO support, leading to the formation of GO/organosilica hybrid material. In comparison with the pristine GO, the ^{13}C CP MAS NMR spectrum of NH_2-GO-2 displayed three additional resonance signals at 14, 27, and 47 ppm, corresponding to C1, C2, and C3 atoms in the aminopropyl functional group,[24] confirming that the molecular structure of organic amino groups on the GO surface could be well-retained. Moreover, the peak intensity of two signals at 65 and 75 ppm remarkably decreased due to the reaction between epoxy or hydroxyl groups on the edge of GO and triethoxy groups of 3-aminopropyltriethoxysilane, in good accordance with the FTIR characterization. Furthermore, we also tried to employ ^{15}N CP MAS NMR to directly investigate the molecular structure of the amine group in our representative catalyst NH_2-GO-2. However, we did not collect the valuable information from the obtained ^{15}N NMR spectrum (Supporting Information Figure S1) because the natural abundance of ^{15}N is very low (0.37%).

The XRD patterns in Figure 3 demonstrated that the original sharp diffraction peak at 2θ = 10.2° indicative of the (001)

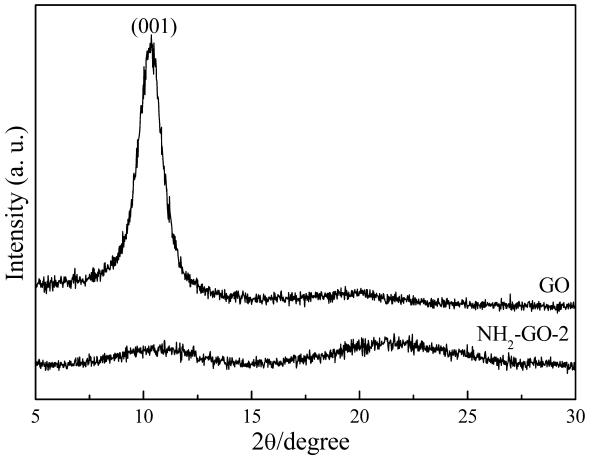

Figure 3. XRD patterns of GO and NH_2-GO-2 samples.

plane of the pristine GO[25] almost completely disappeared and turned into a broad peak in NH_2-GO-2. This revealed that, during the silylation process, the regularly aggregated GO sheets were efficiently exfoliated to basal sheets bridged with amine groups,[26] corresponding to the transformation from

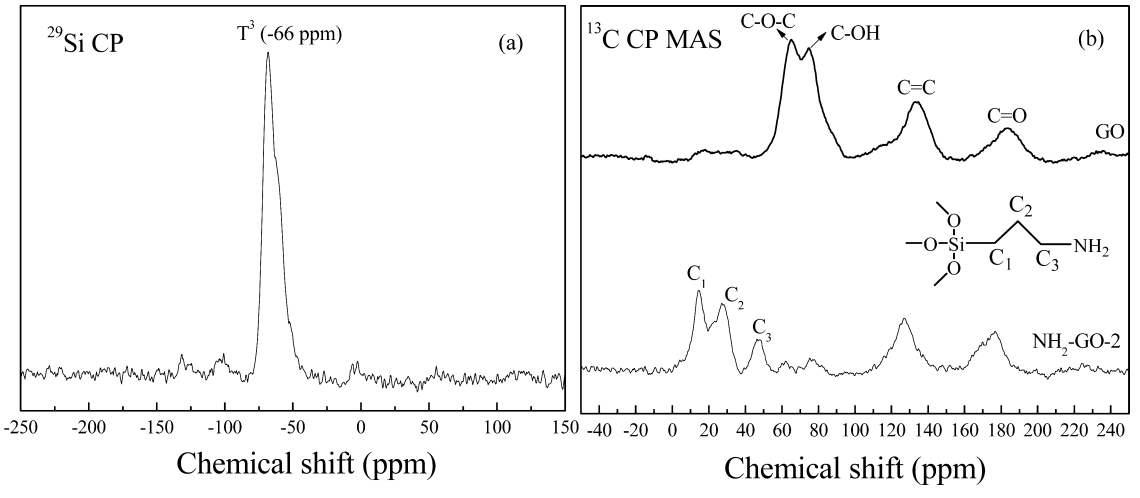

Figure 2. ^{29}Si CP NMR of NH_2-GO-2 (a) and ^{13}C CP MAS NMR of GO and NH_2-GO-2 samples (b).

dx.doi.org/10.1021/cs400761r | ACS Catal. 2014, 4, 394−401

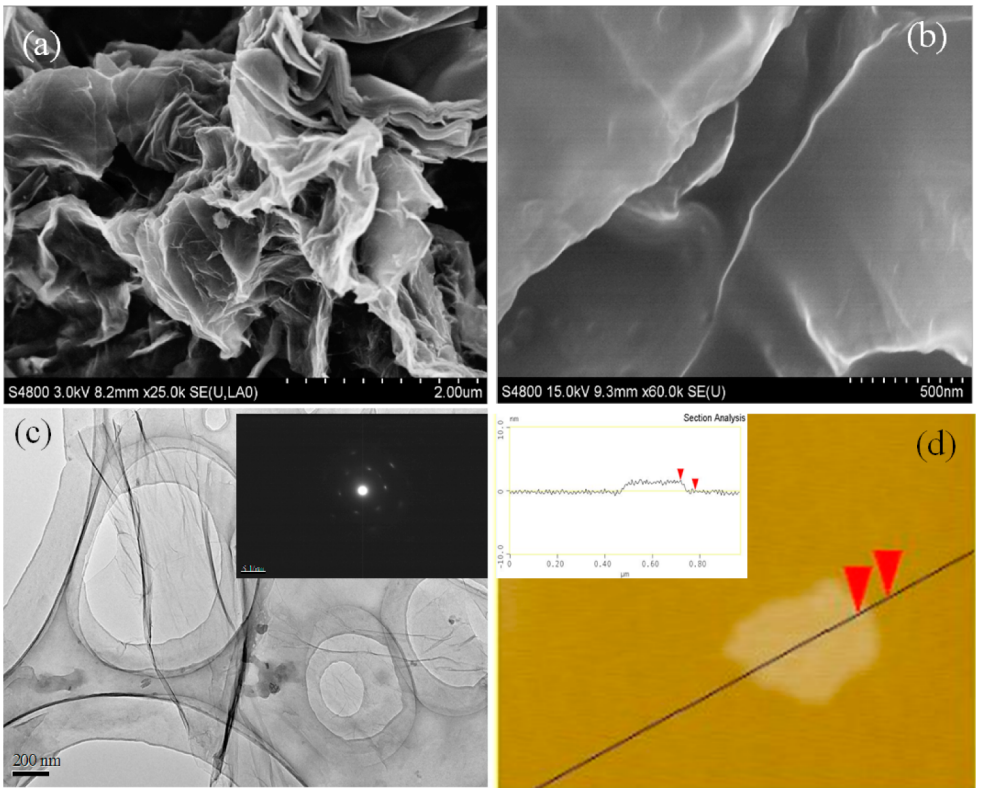

Figure 4. SEM images of GO (a) and NH_2-GO-2 (b), TEM image (c) and AFM image (d) of NH_2-GO-2 (c). The insets in (c) and (d) are the SAED image and the line scan profile of the NH_2-GO-2 flake.

crystalline state to amorphous state. As shown in Figure 4a,b, the SEM images demonstrated that the amine functionalization of GO resulted in the decrease in the degree of sheet aggregation. Meanwhile, the TEM image of NH_2-GO-2 (Figure 4c) confirmed that the amino-silylation caused no significant damage to the GO sheet structure, and the attached selected area electron diffraction (SAED) pattern displayed only diffraction rings characteristic of amorphous state, which was consistent with XRD characterization. Furthermore, the AFM image of NH_2-GO-2 in Figure 4d displayed irregular sheets with an average thickness around 1.5 nm (see the attached line scan profile of the NH_2-GO-2 flake). Taking into account that the thickness of single-layer graphene was about 0.34 nm,[27] we concluded that the enhanced sheet thickness observed from NH_2-GO-2 (1.5 nm) was possibly ascribed to the multiple layers bridged with organic amine groups.

Catalytic Performances. Table 2 summarizes the catalytic performances of NH_2-GO in one-pot cascade reactions containing sequential acetal hydrolysis and Knoevenagel condensation. First, it was found that NH_2-GO-2 catalyst displayed absolute selectivity toward (*E*)-ethyl-2-cyano-3-phenylacrylate product regardless of the reaction conditions. We investigated the catalyst loading and reaction temperature in the NH_2-GO-2-catalyzed one-pot cascade reaction. The benzaldehyde dimethyl acetal conversion increased with the amount of the NH_2-GO-2 catalyst added in the reaction system. Slight diffusion limit was present because the increasing rate of conversion was slightly lower than that of the catalyst amount. Meanwhile, the conversion also remarkably increased with the increase of reaction temperature, which could be attributed to the enhanced molecular motions. The result revealed that NH_2-GO-2 catalyst could obtain high yield (95%) and excellent

Table 2. Catalytic Performances of NH_2-GO in One-Pot Cascade Reactions Containing Hydrolysis and Knoevenagel Condensation[a]

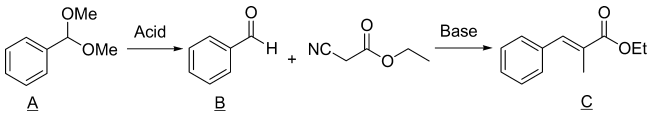

A B C

catalyst	N content (mmol)	*T* (°C)	conversion of A (%)	yield of B (%)	yield of C (%)
NH_2-GO-2	0.040	80	95	0	95
NH_2-GO-2	0.020	30	35	0	35
NH_2-GO-2	0.040	30	47	0	47
NH_2-GO-2	0.080	30	66	0	66
NH_2-GO-2	0.020	60	52	0	52
NH_2-GO-2	0.040	60	74	0	74
NH_2-GO-2	0.080	60	90	0	90
NH_2-GO-2	0.020	80	66	0	66
NH_2-GO-1	0.040	80	95	29	66
NH_2-GO-3	0.040	80	89	2	87

[a]Reaction conditions: benzaldehyde dimethyl acetal (0.50 mmol), ethyl cyanoacetate (0.60 mmol), toluene (5.0 mL), deionized water (50 μL), 3.0 h.

selectivity (100%) with 0.04 mmol N loading at 80 °C for 3.0 h. Next, we compared the catalytic reactivity for NH_2-GO catalyst with different amine content. It was found that the yield of (*E*)-ethyl-2-cyano-3-phenylacrylate first increased and then decreased with the increase of N loading from 0.53 to 1.0 to 2.3 wt %, corresponding to NH_2-GO-1, NH_2-GO-2, and NH_2-GO-3 catalysts, respectively. For NH_2-GO-1 catalyst, it displayed high catalytic reactivity in the acetal hydrolysis reaction. However, the decreased conversion of the Knoevenagel

dx.doi.org/10.1021/cs400761r | ACS Catal. 2014, 4, 394−401

condensation reaction caused the unsatisfactory yield. Moreover, NH_2-GO-3 catalyst also displayed inferior catalytic performance owing to the reduced conversion of the acetal hydrolysis reaction. To explain this phenomenon, we measured the amounts of acidic site and basic site of the NH_2-GO catalysts by NH_3-TPD (Figure S2) and elemental analysis, respectively. As shown in Table 3, for NH_2-GO-1 catalyst, the highest acidic site amount led to the good conversion in the first step, and meanwhile, the lowest basic site amount caused the uncompleted conversion in the Knoevenagel reaction. It could be attributed that the high dispersion of amine active sites with long distance between each other was unfavorable to this second cross-coupling reaction between benzaldehyde and ethyl cyanoacetate adsorbed on two neighboring active sites. However, very high N loading in the NH_2-GO-3 catalyst was also harmful for the present reaction due to the decreased acidic site amount and the enhanced steric hindrance for the diffusion and adsorption of reactant molecules onto amine active sites.

Table 3. Active Site Amount of Different Amine-Functionalized Catalysts

sample	acidic site amount (mmol/g)	basic site amount (mmol/g)
NH_2-GO-1	2.59	0.378
NH_2-GO-2	1.66	0.714
NH_2-GO-3	1.03	1.64
NH_2-AC	1.02	0.714
NH_2-SBA-15	0.234	0.786
NH_2-Al_2O_3	0.633	0.928

To furthermore understand the unique catalytic performance of NH_2-GO-3 catalyst, several control experiments were carried out in the same reaction conditions (Table 4). The pristine GO could efficiently catalyze the hydrolysis of A to B, but it could not catalyze the subsequent Knoevenagel condensation to produce target product (C) due to the absence of base catalyst, revealing that the carboxylic acids on the edges of GO participated in the acetal hydrolysis reaction. Similarly, no significant reaction occurred by using pure propylamine as a homogeneous catalyst since it could not catalyze the hydrolysis of A to B due to the absence of acid catalyst. Interestingly, we found that the physical mixture of GO and propylamine exhibited significant efficiency decrease in both the first hydrolysis of A to B and the subsequent Knoevenagel condensation. The increased amount of GO sample led to the enhanced conversion of the acetal hydrolysis reaction and also caused the decreased catalytic efficiency in the Knoevenagel reaction. This phenomenon could be attributed to the cross-poisoning effects between acid and base catalysts due to the neutralization reaction between carboxyl acid on the GO sheets and free propylamine. We furthermore tested the catalytic activity of the acidified NH_2-GO-2 (NH_2-GO-2-A) and basified NH_2-GO-2 (NH_2-GO-2-B) catalysts. As shown in Table 4, NH_2-GO-2-B catalyst lost its activity completely because it could not catalyze the first step reaction. In the other case, NH_2-GO-2-A catalyst preceded the hydrolysis reaction well; however, the remarkable decrease yield confirmed that the acidified process destroyed the basic sites. Also, the mixture of GO and NH_2-GO-2-B catalysts showed the reduced catalytic efficiency in comparison with NH_2-GO-2 catalyst, which could be attributed to the enhanced transfer limitation owing to the mutual layer−layer interaction between GO and NH_2-GO-2-B samples. These results demonstrated that acidic and basic sites existed separately in a single flake of NH_2-GO-2 catalyst, resulting in the excellent catalytic activity.[28] To explore the mechanism for the catalyst behavior of NH_2-GO-2 catalyst, we changed toluene solvent to protic ethanol solvent, and the result showed that NH_2-GO-2 catalyst displayed almost the same catalytic reactivity for the acetal hydrolysis reaction (Table 4). However, it exhibited decreased catalytic reactivity for the Knoevenagel reaction, which was maybe due to the formation of the NH_3^+ group resulting from a H^+ proton in the carboxylic acid groups.[29] Thus, this phenomenon could be attributed to the combination of NH_2-GO-2 catalyst and anhydrous toluene that could not shuttle the proton effectively and created isolated regions of acid−base functionality that reacted independently with different reactants.[30]

Table 4. Catalytic Performances in "One-Pot" Cascade Reactions Containing Hydrolysis and Knoevenagel Condensation[a]

catalyst	conversion of A (%)	yield of B (%)	yield of C (%)
GO[b]	94	94	0
$C_3H_7NH_2$[c]	0	0	0
GO + $C_3H_7NH_2$[d]	23	5	18
GO + $C_3H_7NH_2$[e]	56	7	49
GO + $C_3H_7NH_2$[f]	73	22	51
NH_2-GO-2-A	99	71	28
NH_2-GO-2-B	0	0	0
GO + NH_2-GO-2-B	82	12	70
NH_2-GO-2[g]	96	26	70
NH_2-AC	36	8	28
NH_2-SBA-15	44	13	31
NH_2-Al_2O_3	52	6	46

[a]Reaction conditions: benzaldehyde dimethyl acetal (0.50 mmol), ethyl cyanoacetate (0.60 mmol), a catalyst containing 0.040 mmol N content, toluene (5.0 mL), deionized water (50 μL), 80 °C, 3.0 h. [b]With 50 mg of GO. [c]With 0.040 mmol $C_3H_7NH_2$. [d]With 25 mg of GO and 0.040 mmol $C_3H_7NH_2$. [e]With 50 mg of GO and 0.040 mmol $C_3H_7NH_2$. [f]With 75 mg of GO and 0.040 mmol $C_3H_7NH_2$. [g]Using 5 mL of ethanol instead of toluene as solvent.

To furthermore demonstrate the advantage of NH_2-GO-2 catalyst, we compared the performances of different NH_2-functionalized catalysts in the one-pot cascade reaction. Compared to NH_2-AC, NH_2-SBA-15, and NH_2-Al_2O_3 with almost the same N loadings (∼1.0 wt %), the NH_2-GO-2 exhibited much higher activity in either the first acetal hydrolysis or the subsequent Knoevenagel condensation (Table 4), leading to the high yield and absolute selectivity toward target product C, which could also be confirmed by the reaction profiles of the Knoevenagel reaction (Figure S3). As shown in Figure 5, the XPS analysis demonstrated that NH_2-GO-2, NH_2-AC, and NH_2-SBA-15 catalysts showed similar features and chemical microenvironment of base active sites, corresponding to the principal peak with binding energy around 399.1 eV characteristic of amine groups.[31] Unlike either the NH_2-AC or the NH_2-SBA-15, the NH_2-GO-2 displayed a well-resolved peak at binding energy around 289.1 eV indicative of the O−C═O bond, indicating the presence of carboxylic acid groups (see Scheme 1).[32] The NH_3-TPD curves in Figure 6 revealed that, besides the desorption peak at 550 °C due to the decomposition of aminopropyl groups terminally bonded to the supports, the NH_2-GO-2 displayed much stronger

dx.doi.org/10.1021/cs400761r | ACS Catal. 2014, 4, 394−401

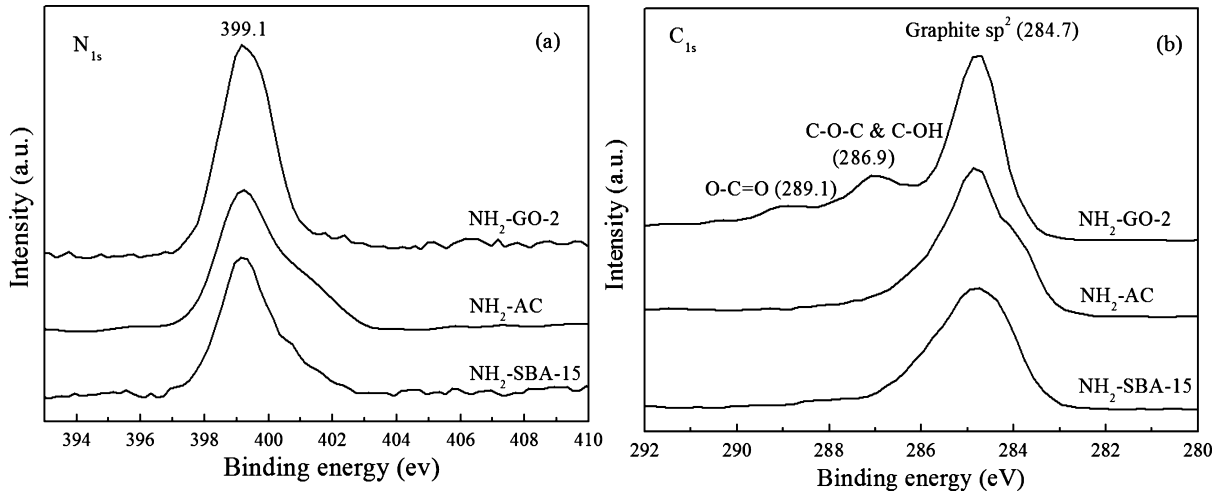

Figure 5. XPS spectra of NH_2-GO-2, NH_2-AC, and NH_2-SBA-15 samples (a, N1s; b, C1s).

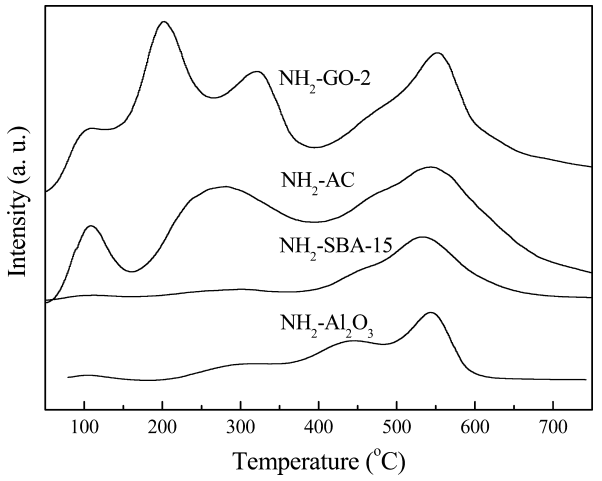

Figure 6. NH_3-TPD profiles of NH_2-GO, NH_2-AC, and NH_2-SBA-15 samples.

desorption peaks than either NH_2-AC, NH_2-SBA-15, or NH_2-Al_2O_3 in the temperature range from 150 to 400 °C, implying the presence of more carboxylic acid sites,[33] which could sufficiently account for its higher activity.[34] The quantitative results (Table 3) demonstrated that NH_2-GO-2 had the highest acidic site amount in comparison with NH_2-AC, NH_2-SBA-15, and NH_2-Al_2O_3 catalysts.[35] Besides, the SEM and TEM images (Figure S2) revealed that NH_2-AC and NH_2-SBA-15 were present in three-dimensional shapes with microporous and mesoporous structure, respectively. However, the NH_2-GO-2 displayed two-dimensional sheets, which favored diffusion and adsorption of reactant molecules onto the active sites.[36] Although the NH_3-TPD curves in Figure 6 revealed that the NH_2-AC contained much more acid sites than the NH_2-SBA-15, it still exhibited lower activity than the NH_2-SBA-15, possibly due to the enhanced diffusion limit in irregular micropores than that in ordered mesoporous channels. Moreover, Figure 7 revealed that both the NH_2-AC and the NH_2-SBA-15 easily settled down from the solution, while the NH_2-GO-2 still had high dispersion in solution within 1.0 h owing to the unique two-dimensional structure, which also promoted catalytic activity by enhancing the contacting probability between the reactant molecules and the catalyst. To demonstrate this advantage of the combination of suitable carboxylic acid intensity and unique two-dimension structure of the NH_2-GO-2 catalyst, we calculated the apparent activation energy over different catalysts. The plots of the concentration of benzaldehyde dimethyl acetal versus reaction time and the Arrhenius plots for NH_2-GO-2, NH_2-AC, and NH_2-SBA-15 catalysts in the temperature range from 60 to 80 °C are shown in Figures S5−S7. The results indicated that the overall reaction

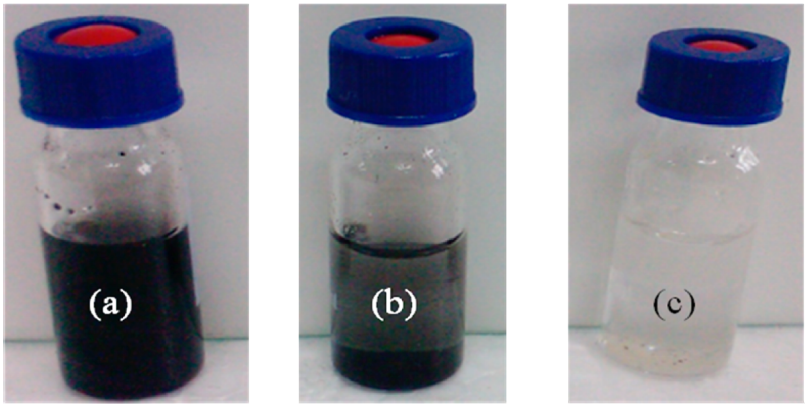

Figure 7. Picture of NH_2-GO (a), NH_2-AC (b), and NH_2-SBA-15 (c) dispersed in toluene after ultrasound for 10 min and the following static settlement for 1.0 h.

dx.doi.org/10.1021/cs400761r | ACS Catal. 2014, 4, 394−401

might be a second-order reaction of benzaldehyde dimethyl acetal since the calculated concentrations of benzaldehyde dimethyl acetal $(1/C_t)$ in the time courses increased linearly with the reaction time (t) according to the reaction rate equation, $1/C_t = kt + 1/C_0$.[37] Accordingly, the calculated activation energies for NH_2-GO-2, NH_2-AC, and NH_2-SBA-15 catalysts were 63.9, 67.3, and 66.6 kJ/mol, respectively. Thus, the lowest activation energy for NH_2-GO-2 in this cascade reaction was responsible for its highest catalytic efficiency.

To ensure that the catalytic activity originated from the NH_2-GO-2 sample other than from a dissolved amine group either from the absorbed amine or from catalyst leaching, the following procedure proposed by Sheldon et al. was carried out.[38] After reaction for 1.5 h, where the conversion exceeded 45% in this cascade reaction, the mixture was filtered to remove the solid catalyst and then allowed the mother liquor to react for another 3.0 h under the same reaction conditions. No significant acetal hydrolysis nor increased yield of (*E*)-ethyl-2-cyano-3-phenylacrylate was observed, demonstrating that the active species were not the dissolved amine leached from NH_2-GO-2 catalyst. Therefore, it was reasonable to suggest that the present catalysis was heterogeneous in nature.

An important merit of heterogeneous catalyst is that they could be conveniently recycled and reused.[39] As shown in Figure 8, the NH_2-GO-2 catalyst could be used repetitively for

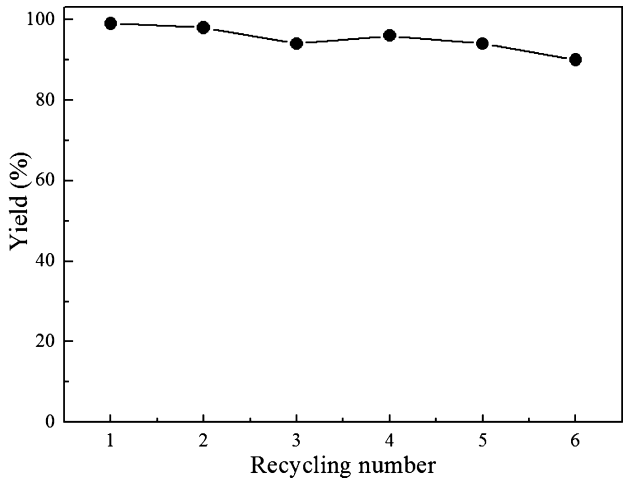

Figure 8. Recycling tests of NH_2-GO-2 catalyst during deacetalization−Knoevenagel cascade reaction. Reaction condition is shown in Table 2.

at least six times without significant decrease in the yield of (*E*)-ethyl-2-cyano-3-phenylacrylate. On one hand, the elemental analysis demonstrated that the N loading in NH_2-GO-2 catalyst remained almost the same (1.0 wt %) after being reused six times, implying the excellent stability against amine leaching owing to its covalent bond with the GO sheets. On the other hand, TEM image (Figure S8) revealed that the NH_2-GO-2 well-preserved its original morphology after being reused six times, showing excellent hydrothermal stability against either the catalyst aggregation or structural damage.

CONCLUSIONS

In summary, this work developed a novel acid−base bifunctional catalyst by grafting amine groups onto GO sheets through a facile one-step silylation approach, which exhibited high activity and selectivity in one-pot cascade reactions comprising sequential acetal hydrolysis and Knoevenagel condensation owing to the enriched surface carboxylic acid sites and the diminished diffusion limit on the unique two-dimensional sheets as well as the high catalyst dispersion in the liquid phase. Other acid−base bifunctional catalysts could be further designed in this way and could be used in various one-pot cascade reactions catalyzed by both acid and base catalysts, which might offer a general route for simple and green organic synthesis with high efficiencies.

ASSOCIATED CONTENT

Supporting Information

This material is available free of charge via the Internet at http://pubs.acs.org.

AUTHOR INFORMATION

Corresponding Authors

*Tel: +86-21-64322272. Fax: +86-21-64322272. E-mail: zhangfang@shnu.edu.cn.

*Tel: +86-21-64322272. Fax: +86-21-64322272. E-mail: hexing-li@shnu.edu.cn.

Notes

The authors declare no competing financial interest.

ACKNOWLEDGMENTS

This work is supported by Natural Science Foundation of China (21107071 and 51273112), PCSIRT (IRT1269) and Shanghai Government (10dj1400100 and 13QA1402800).

REFERENCES

(1) Clardy, J.; Walsh, C. *Nature* **2004**, *432*, 829.
(2) Ambrosini, L. M.; Lambert, T. H. *ChemCatChem* **2010**, *2*, 1373.
(3) Albrecht, Ł.; Jiang, H.; Jørgensen, K. A. *Angew. Chem., Int. Ed.* **2011**, *50*, 2.
(4) Tietze, L. F.; Brasche, G.; Gericke, K. M. *Domino Reactions in Organic Synthesis*; Wiley-VCH: Weinheim, Germany, 2006.
(5) (a) Shibasaki, M.; Yamamoto, Y. *Multimetallic Catalysts in Organic Synthesis*; Wiley-VCH: Weinheim, Germany, 2007. (b) Ramachary, D. B.; Jain, S. *Org. Biomol. Chem.* **2011**, *9*, 1277.
(6) Benaglia, M. *Recoverable and Recyclable Catalysts*; Wiley-VCH: Chichester, UK, 2009.
(7) Climent, M.; Corma, A.; Iborra, S. *Chem. Rev.* **2011**, *111*, 1072.
(8) Broadwater, S. J.; Roth, S. L.; Price, K. E.; Kobašlijia, M.; McQuade, D. T. *Org. Biomol. Chem.* **2005**, *3*, 2899.
(9) (a) Voit, B. *Angew. Chem., Int. Ed.* **2007**, *46*, 4238. (b) Motokura, K.; Tada, M.; Iwasawa, Y. *J. Am. Chem. Soc.* **2009**, *131*, 7944. (c) Rodionov, V.; Gao, H. F.; Scroggins, S.; Unruh, D. A.; Avestro, A. J.; Fréchet, J. M. J. *J. Am. Chem. Soc.* **2010**, *132*, 2570. (d) Shang, F. P.; Liu, H.; Sun, J. R.; Liu, B.; Wang, C. H.; Guan, J. Q.; Kan, Q. B. *Catal. Commun.* **2011**, *12*, 739. (e) Wang, C. H.; Shang, F. P.; Yu, X. F.; Guan, J. Q.; Kan, Q. B. *Appl. Surf. Sci.* **2012**, *258*, 6846. (f) Li, P.; Cao, C. Y.; Chen, Z.; Liu, H.; Yu, Y.; Song, W. G. *Chem. Commun.* **2012**, *48*, 10541. (g) Shang, F. P.; Sun, J. R.; Wu, S.; Yang, Y.; Kan, Q.; Guan, J. Q. *Microporous Mesoporous Mater.* **2010**, *134*, 44. (h) Shang, F. P.; Sun, J. R.; Liu, H.; Wang, C. H.; Guan, J. Q.; Kan, Q. B. *Mater. Res. Bull.* **2012**, *47*, 801. (i) Merino, E.; Verde-Sesto, E.; Maya, E. M.; Iglesisa, M.; Sánchez, F.; Corma, A. *Chem. Mater.* **2013**, *25*, 981. (j) Xia, S. X.; Nie, R. F.; Lu, X. Y.; Wang, L. N.; Chen, P.; Hou, Z. Y. *J. Catal.* **2012**, *296*, 1−11.
(10) Gelman, F.; Blum, J.; Avnir, D. *J. Am. Chem. Soc.* **2002**, *124*, 14460.
(11) (a) Margelefsky, E. L.; Zeidan, R. K.; Davis, M. E. *Chem. Soc. Rev.* **2008**, *37*, 1118. (b) Shylesh, S.; Thiel, W. R. *ChemCatChem* **2011**, *3*, 278.

(12) (a) Shylesh, S.; Wagener, A.; Seifert, A.; Ernst, S.; Thiel, W. R. *Angew. Chem., Int. Ed.* **2010**, *49*, 184. (b) Huang, Y. L.; Xu, S.; Lin, V. S. *Angew. Chem., Int. Ed.* **2011**, *50*, 661.
(13) Motokura, K.; Tada, M.; Iwasawa, Y. *J. Am. Chem. Soc.* **2007**, *129*, 9540.
(14) Motokura, K.; Tada, M.; Iwasawa, Y. *Chem.—Asian J.* **2008**, *3*, 1230.
(15) Allen, M. J.; Tung, V. C.; Kaner, R. B. *Chem. Rev.* **2010**, *110*, 132.
(16) (a) Pyun, J. *Angew. Chem., Int. Ed.* **2011**, *50*, 46. (b) Hong, S. M.; Kim, S. H.; Lee, K. B. *Energy Fuels* **2013**, *27*, 3358. (c) Fu, Y.; Zhang, J. W.; Liu, H.; Hiscox, W. C.; Gu, Y. *J. Mater. Chem. A* **2013**, *1*, 2663.
(17) Dreyer, D. R.; Bielawski, C. W. *Chem. Sci.* **2011**, *2*, 1233.
(18) Jia, H. P.; Dreyer, D. R.; Bielawski, C. W. *Adv. Synth. Catal.* **2011**, *53*, 528.
(19) Zhao, D.; Feng, J.; Huo, Q.; Fredrickson, G. H.; Stucky, G. D. *Science* **1998**, *279*, 548.
(20) Yang, X.; Wang, X.; Yang, J.; Li, J.; Wan, L. *Chem. Phys. Lett.* **2013**, *570*, 125.
(21) Valentini, L.; Bon, S. B.; Monticelli, O.; Kenny, J. M. *J. Mater. Chem.* **2012**, *22*, 6213.
(22) Maria Chong, A. S.; Zhao, X. S. *J. Phys. Chem. B* **2003**, *107*, 12650.
(23) Wan, Y.; Zhang, F.; Lu, Y. F.; Li, H. X. *J. Mol. Catal. A* **2007**, *267*, 165.
(24) (a) Brunelli, N. A.; Didas, S. A.; Venkatasubbaish, K.; Jones, C. W. *J. Am. Chem. Soc.* **2012**, *134*, 13950. (b) Hou, S. F.; Kasner, M. L.; Su, S. J.; Patel, K.; Cuellari, R. *J. Phys. Chem. C* **2010**, *114*, 14915−14921.
(25) Wang, H. L.; Robinson, J. T.; Diankov, G.; Dai, H. J. *J. Am. Chem. Soc.* **2010**, *132*, 3270.
(26) Chen, S.; Zhu, J. W.; Wu, X. D.; Han, Q. F.; Wang, X. *ACS Nano* **2010**, *4*, 2822.
(27) Geim, K.; Novoselov, K. S. *Nat. Mater.* **2007**, *6*, 183.
(28) Phan, N. T. S.; Gill, C. S.; Nguyen, J. S.; Zhang, Z. J.; Jones, C. W. *Angew. Chem., Int. Ed.* **2006**, *45*, 2209.
(29) Boukhvalov, D. W.; Dreyer, D. R.; Bielawski, C. W.; Son, Y. W. *ChemCatChem* **2012**, *4*, 1844.
(30) Merino, E.; Verde-Sesto, E.; Maya, E. M.; Iglesisa, M.; Sánchez, F.; Corma, A. *Chem. Mater.* **2013**, *25*, 981−988.
(31) (a) An, Y. Q.; Chen, M.; Xue, Q. J.; Liu, W. M. *J. Colloid Interface Sci.* **2007**, *311*, 507. (b) Goonasekera, C. S.; Jack, K. S.; Copper-White, J. J.; Grøndahl, L. *J. Mater. Chem. B* **2013**, *1*, 5842.
(32) Yuan, C. F.; Chen, W. F.; Yan, L. F. *J. Mater. Chem.* **2012**, *22*, 7456.
(33) Wang, S. P.; Zhao, L. F.; Wang, W.; Zhao, Y. J.; Zhang, G. L.; Ma, X. B.; Gong, J. L. *Nanoscale* **2013**, *5*, 5582.
(34) Zeidan, R. K.; Davis, M. E. *J. Catal.* **2007**, *247*, 379.
(35) Gong, L. F.; Lu, Y.; Ding, Y. J.; Lin, R. H.; Li, J. W.; Dong, W. D.; Wang, T.; Chen, W. M. *Appl. Catal. A: Gen.* **2010**, *390*, 119.
(36) Li, C. *Catal. Rev.* **2004**, *46*, 419.
(37) Xia, S. X.; Nie, R. F.; Lu, X. Y.; Wang, L. N.; Chen, P.; Hou, Z. Y. *J. Catal.* **2012**, *296*, 1−11.
(38) Sheldon, R. A.; Wallau, M. I.; Arends, W. C.; Schuchardt, E. U. *Acc. Chem. Res.* **1998**, *31*, 485.
(39) Thomas, A. *Angew. Chem., Int. Ed.* **2010**, *49*, 8328.